Supplementary Information of

"Giant surface potentials in organic films enable electrode-free self-driven water droplets"

Tsuyoshi Tsujioka[1]*, Hiroyuki Kawashima[2], Kenji Koike[2], Naoki Matsumoto[2], Junwei Shen[3], and Shinichiro Nakamura[3]**

[1]Division of Math, Sciences, and Information Technology in Education, Osaka Kyoiku University, 4-698-2, Asahigaoka, Kashiwara, Osaka 582-8582, Japan

[2]Tosoh Corp., 2743-1, Hayakawa, Ayase, Kanagawa 252-1123, Japan

[3]Research and Education Institute for Semiconductors and Informatics, Kumamoto University, 2-39-1, Kurokami, Chuo, Kumamoto 860-8555, Japan

*E-mail: tsujioka@cc.osaka-kyoiku.ac.jp

**Email: shindon@dsk.kumamoto-u.ac.jp

Alq3 powder attracted to strong electric field gradient and its fluorescence

Figure S1 demonstrates that dielectric Alq3 powder is attracted to regions with strong electric field gradients and emits intense fluorescence under UV illumination. When a voltage of 100 V is applied to a silver (Ag) electrode with a 150-μm gap, and Alq_3 powder is sprinkled and subsequently shaken off, the powder accumulates in the gap and emits strong fluorescence. Panel (b) presents a photograph of the experimental results: the left image shows the outcome without voltage, while the right image shows the result with voltage applied. Under applied voltage, a fluorescent line appears along the electrode gap.

a

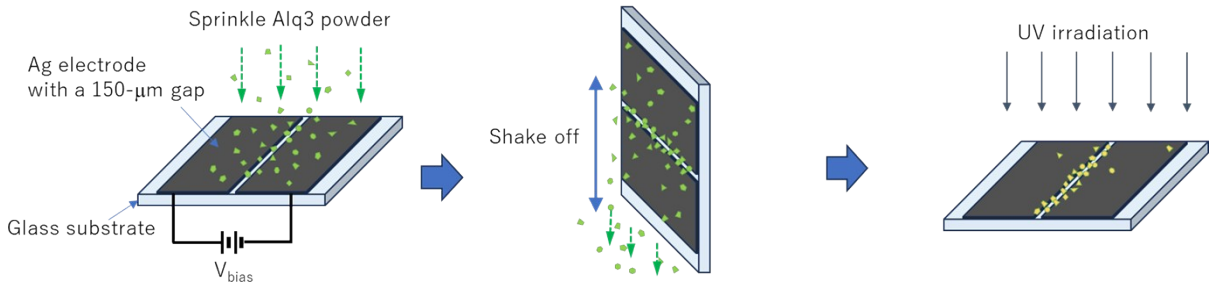

b

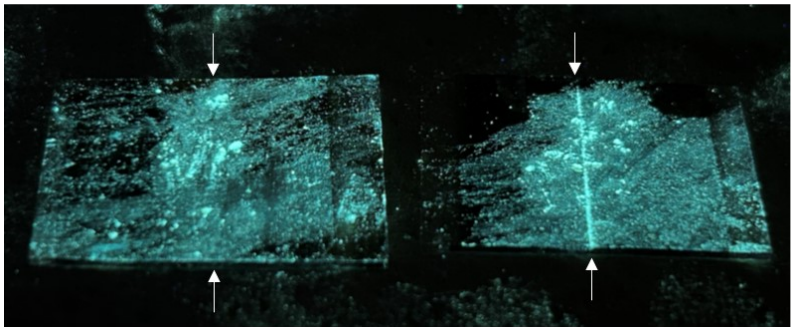

Fig. S1 (a) Schematic diagram of an experiment in which Alq3 powder is attracted to a location with a large electric field gradient. (b) Left: no voltage applied, right: 100 V. The white arrows indicate the location of the gap.

Surface potential measuring device using electrostatic induction

Figure S2a illustrates the experimental setup used to measure the surface potential in this study. A portable surface potential measurement device (KSD-3000, Kasuga Electric Co., Ltd.) was placed inside an electrostatic shielding container and positioned such that the distance between the measurement sample surface and the probe was 10 mm.

Figure S2b present a model of the measurement system, specifically focusing on the effects of applying a GSP film to a dielectric substrate, such as glass, on surface potential measurements. The system is modeled as two parallel capacitors: the GSP layer acts as a constant voltage source (V_x), while the electrodes form two capacitors with top and bottom earth electrodes. V_x can be derived from the measurable V_m. For a glass substrate with a thickness of 1.0 mm and a relative permittivity of approximately 5, the error is around 2%, which is smaller than the measurement error and can be considered negligible. Calibration of this measurement device was conducted using the known GSP measurements of the Alq3 film.

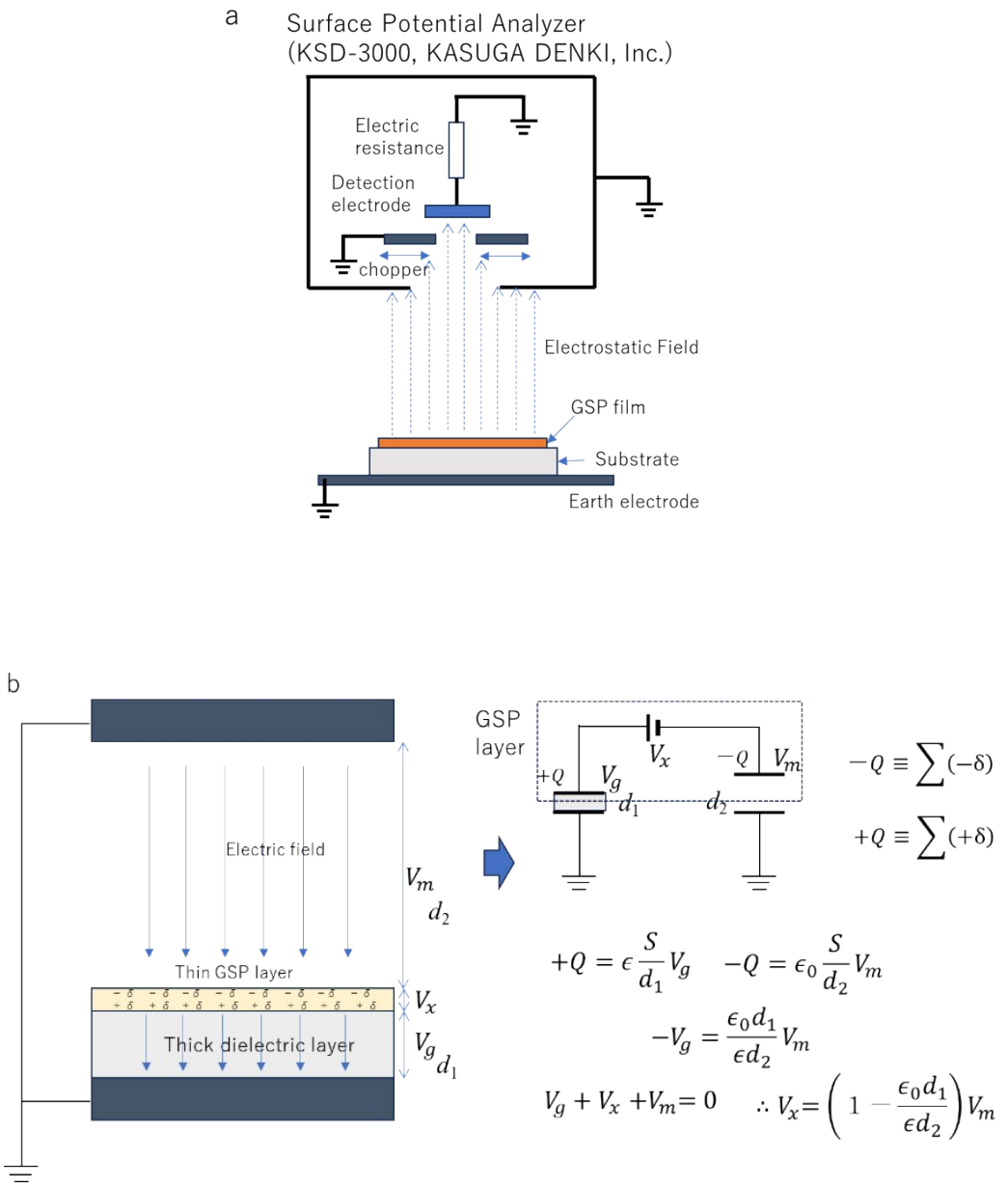

Fig. S2 (a) Surface potential measuring device using electrostatic induction. (b) Concept of surface potential measurement when the substrate is an insulator such as a glass substrate and two capacitor model of measurement system.

Decrease in surface potential due to contact with water

The reduction in surface potential upon contact with water was measured using the procedure shown in Figure S3. The surface potential of a PTAA film, formed by vapor deposition on a glass or Si substrate, was first recorded. Water was then carefully applied to the PTAA surface and subsequently removed without contacting the substrate, after which the surface potential was measured again. This procedure was designed to mimic conditions similar to those experienced when a water droplet is deposited onto a surface. The results are presented in Figure 1c. When water contacts the substrate, the residual surface potential either decreases to near zero or fluctuates substantially, due to the inflow and outflow of charges via the substrate.

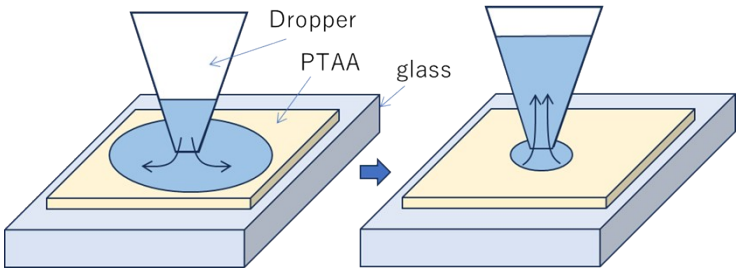

Fig. S3 Contact method between PTAA surface and water

Driving Force Illustration of Water-Droplet Movement in Fig. 1d

Figure S4a illustrates the driving force behind water droplet movement shown in the left panel of Fig. 1d. As a droplet approaches the edge of the PTAA film, it is pulled back by the attractive force from the opposing surface potential, similar to being reflected.

Figure S4b shows an illustration of the driving force in the right panel of Figure 1e. When droplet A (2 in Fig. 1e) approaches another droplet B (1 in Fig. 1e), the driving force that should attract droplet A is reduced due to the small magnitude of the surface potential at the droplet B-substrate interface. As a result, droplet A stops moving. Meanwhile, droplet B is initially stationary because the surface potentials on the left and right sides are balanced. However, as droplet A approaches, this balance is disrupted, generating a driving force that pushes droplet B away from droplet A, causing droplet B to move to the left.

This movement of droplets, first approaching and then separating, clearly indicates that Coulomb repulsion between droplets is not the driving force.

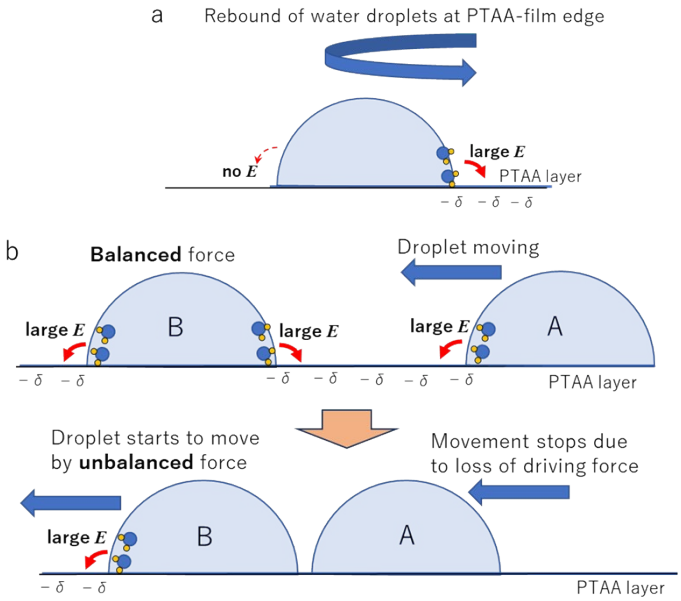

Fig. S4 (a) Driving force illustration on water droplet "reflection" at PTAA film edge. (b) Driving force illustration on water droplet "repulsion" between multiple water droplets like "slow billiards".

Approximate Derivation of Dielectrophoretic Force on Dielectric Droplet

The force acting on a dielectric body in an electric field can be expressed as the surface integral of the Maxwell stress tensor **T**:

$$F = \oint T \cdot n \, dS$$

or equivalently as the volume integral of its divergence:

$$F = \int \nabla \cdot T \, dV.$$

For a linear, isotropic dielectric medium with uniform permittivity ε, the Maxwell stress tensor is given by

$$T = \varepsilon[(E \cdot E)I - E \otimes E].$$

Taking the divergence of the tensor assuming a linear dielectric medium with spatially uniform permittivity ($\nabla\varepsilon = 0$), under electrostatic conditions ($\nabla \times \boldsymbol{E} = 0$), and in the absence of free charges, the force density can be expressed as

$$f = \nabla \cdot T = \frac{\varepsilon}{2}\nabla(E^2),$$

where higher-order terms vanish under the assumption of a homogeneous medium. This expression corresponds to the well-known form of the dielectrophoretic force. Applying this to our conditions (Fig. 3a), the following equation is derived:

$$f = \frac{1}{2}\varepsilon_0(\varepsilon_r - 1)\nabla(E^2) \quad [1]$$

We want to estimate the x-component of the force acting on a dielectric cube (size w) placed in the $x>0$ region, when the potential on the plane $x<0$ is V_0 and on $x>0$ is V ($|V| < |V_0|$). The axis of the cube coincides with the z-axis (Fig. 3a). The potential difference is $\Delta V = |V_0 - V|$. In the

theoretical model shown in Fig. 3a, the electric field strength at coordinate (x, y) in a vacuum (permittivity ε_0) without a dielectric is expressed as

$$|E| \sim \frac{\Delta V}{\pi \sqrt{x^2 + y^2}}$$

(1) The dielectric occupies only the half-sphere in x>0, with relative permittivity ε_r. The thickness of the electric field transition region (skin region) is x_1.

(2) The sharp potential change across the boundary is localized in the skin region. The x-components of electric field at $x = 0$ and $x = x_1$, which has y-dependence, is

$$|E_x(x = 0,\ y)| \sim \frac{\Delta V}{\pi y + x_1}, \quad |E_x(x = x_1, y)| \sim \frac{1}{\varepsilon_r} \frac{\Delta V}{\pi y + x_1}.$$

(3) The gradient of the E_x^2 in the skin region can be approximated as:

$$\frac{|E_x(x = 0,\ y)|^2 - |E_x(x = x_1, y)|^2}{x_1} = \left(\frac{\Delta V}{\pi y + x_1}\right)^2 \left(1 - \frac{1}{{\varepsilon_r}^2}\right) \frac{1}{x_1} \sim \left(\frac{\Delta V}{\pi y + x_1}\right)^2 \frac{1}{x_1},$$

where we used the approximation $1 \gg 1/{\varepsilon_r}^2 \sim 0$. Integrating with $x \in [0, x_1]$, $y \in [0, w]$, and z $\in$ $[0, w]$ gives

$$|F_x| = \frac{\varepsilon_r \varepsilon_0}{2} \int_0^{x1} dx \int_0^{w} dy \int_0^{w} dz \left(\frac{\Delta V}{\pi y + x_1}\right)^2 \frac{1}{x_1} \sim \frac{\varepsilon_r \varepsilon_0}{2} (\Delta V)^2 \frac{w}{\pi x_1}. \quad [2]$$

where we used the approximation $\pi w \gg x_1$.

Relationship between water droplet mobility and Surface roughness Ra

Figure S5 shows the mobility of a water droplet on a PTAA surface as a function of Ra and ΔV. PTAA films were deposited on both a Si substrate or a glass substrate with a larger Ra. In general, a thicker film results in a larger Ra. Even when ΔV is large, if Ra is also large, the water droplet is less likely to move, suggesting the existence of an optimal combination of Ra and ΔV.

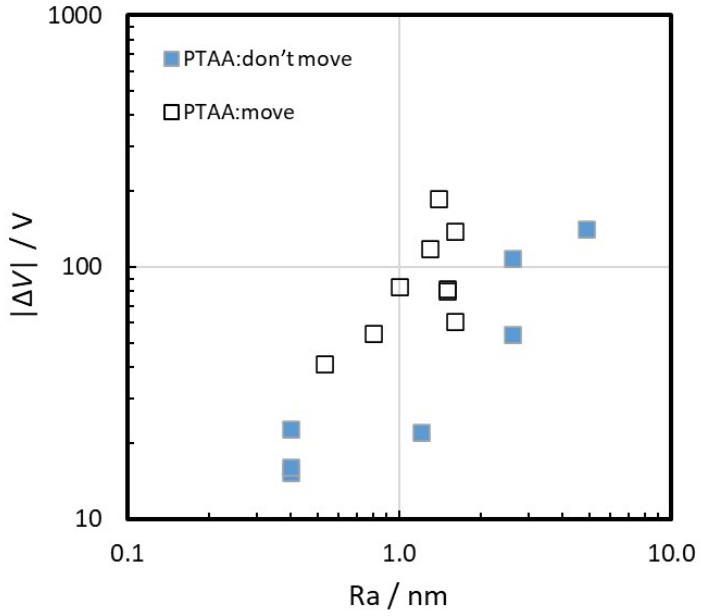

Fig. S5 Mobility of a water droplet on a PTAA surface as a function of Ra and ΔV.

GSP materials

Figure S6 shows molecular structures used in our study. PTAA was newly synthesized at Tosoh corp. All DAEs were synthesized at Kobe Natural Products Chemical Co., Ltd. SPP (product number D5626) was purchased from Tokyo Chemical Industry Co., Ltd.

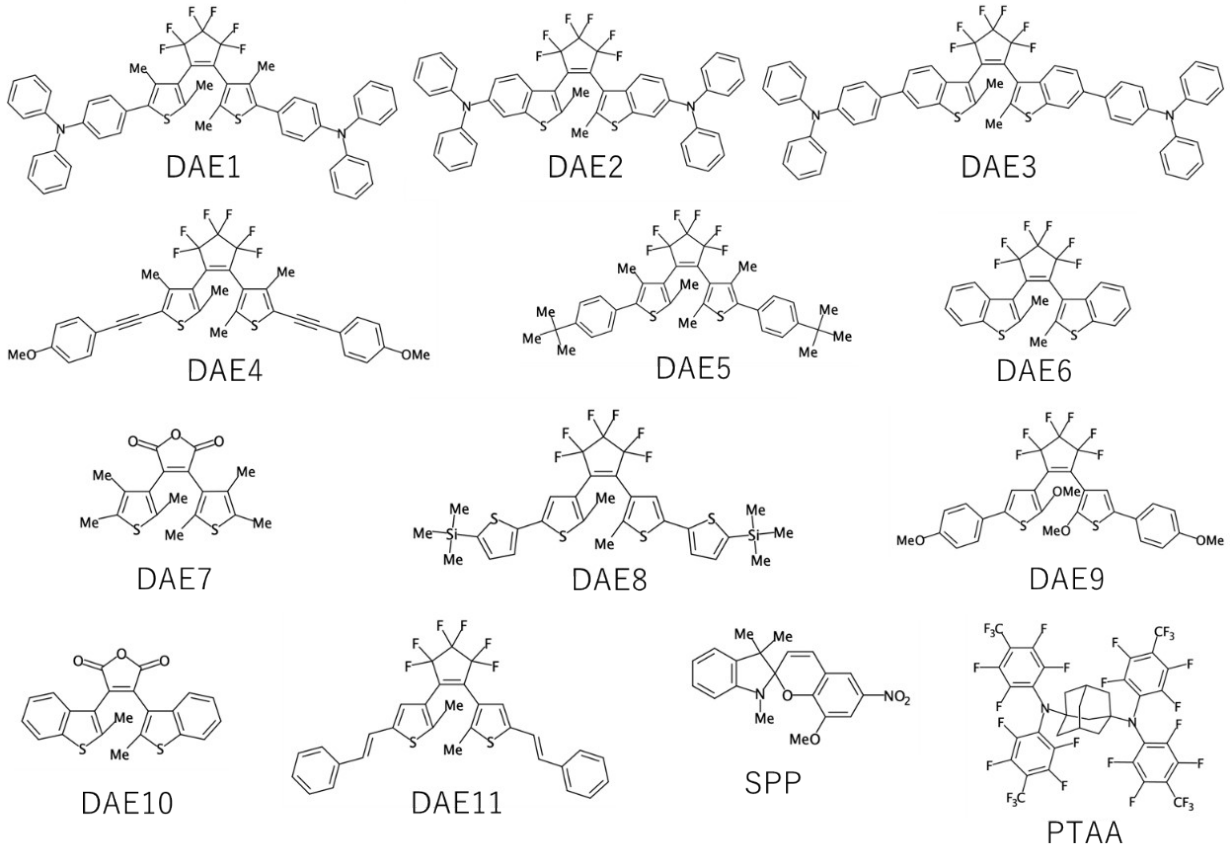

Fig. S6 Molecular structures of materials

Calculated Permanent Molecular Dipole Moment (PDM), Molecular Volumes, and Their Relationship to the Glass Transition Temperature (Tg)

The results of the PDM calculations for the main diarylethenes and PTAA are shown in Fig. S7 and detailed in Table S1. Diarylethenes (DAEs) undergo ring-closing and ring-opening reactions upon photoirradiation. Some molecules exhibit significant changes in PDM during isomerization, while others show minimal changes. All films formed by vacuum deposition were in the ring-open form, a detail that will be discussed further later. The molecular volume was calculated using Gaussian Molar Volume and COSMO-RS Molar Volume. The results of these molecular volume calculations are summarized in Table S2.

$$\text{GSP slope} \equiv \frac{Surface\ potential}{d} = \frac{1}{\varepsilon_r \varepsilon_0} \frac{p\langle cos\theta \rangle}{V_m},$$

where p represents PDM, V_m denotes the molar volume, ε_0 and ε_r correspond to the vacuum and relative permittivity, and d indicates the GSP layer's thickness. The properties of GSP and the correlation between <cosθ> and Tg and other molecular characteristics were investigated (Fig. S9).

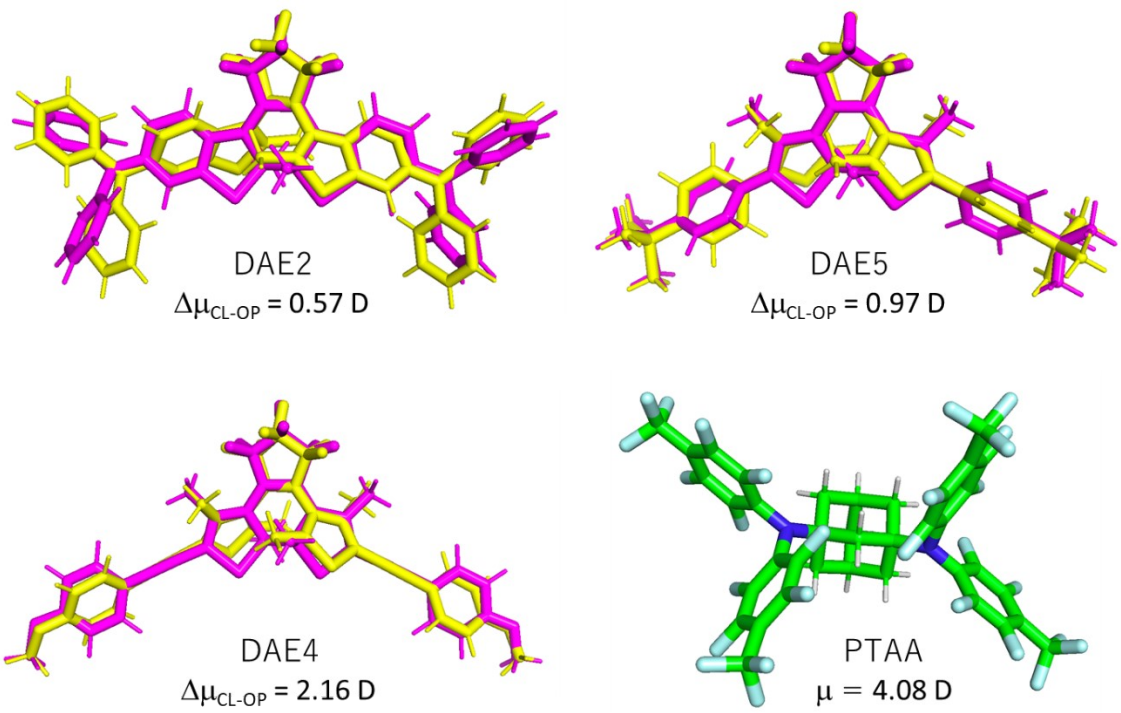

Fig. S7 Examples of PDM calculation for open-ring (yellow) and closed-ring (magenta) forms and PTAA molecule

Table S1 Comparison of PDM calculation results for each molecule with GSP slope. The dipole moments were calculated by Gaussian program at B3LYP/6-311G(d,p) level.

Molecule	GSP / mV/nm	μ (Debye)	
		OPEN	CLOSED
DAE1	-165	4.5549	6.2455
DAE2	-126	3.8201	4.3882
DAE3	-120	4.1883	4.2378
DAE4	-162	6.8063	8.9650
DAE5	39	4.3939	5.3651
DAE6	6	3.6599	2.9734
DAE7	15	4.7934	5.8959
DAE8	2	4.9276	5.9193
DAE9	-3	9.7683	9.7991
DAE10	85	4.8287	4.6017
DAE11	-57	4.4405	5.6844
PTAA	-110	4.0778	
SPP	64	10.1242	4.0386

Table S2 Calculation results of molecular volume and estimated $cos\theta$ values. The molecular volume was predicted by using COSMO-RS model, and the amorphous density at 298.15K was obtained from an average of 10 ns molecular dynamics simulation.

Molecule	Molecular Orientation $< cos\,\theta >$	Molecular Volume V_{mol} [Å^3]	Amorphous Density ρ [g/cm^3]
DAE1	-0.26	1000.96	1.1907 ± 0.0027
DAE2	-0.22	891.48	1.2096 ± 0.0032
DAE3	-0.24	1077.66	1.1500 ± 0.0032
DAE4	-0.14	726.47	1.2479 ± 0.0037
DAE5	0.04	771.28	1.1546 ± 0.0032
DAE6	0.01	486.38	1.3437 ± 0.0043
DAE7	0.01	402.60	1.1950 ± 0.0039
DAE8	0.00	757.11	1.2890 ± 0.0035
DAE9	0.00	636.20	1.3535 ± 0.0037
DAE10	0.05	431.80	1.2792 ± 0.0038
DAE11	-0.05	626.02	1.2691 ± 0.0036
PTAA	-0.15	876.45	1.5475 ± 0.0047
SPP	0.05	414.06	1.1809 ± 0.0035

GSP slopes, PDMs, relative permittivity, and molecular orientations

Figure S8 presents data on T_gs, the GSP slopes, PDM calculation results, relative permittivity, and the mean molecular orientation <cosθ> for vacuum-deposited films of various materials. <cosθ> was determined using following equation.

$$Measured\ surface\ potential = \frac{1}{\varepsilon_0 \varepsilon_r} \frac{p\langle \cos\theta \rangle}{v_m} d ,$$

where p represents PDM, v_m denotes molar volume, ε_0 and ε_r correspond to the permittivity of vacuum and relative permittivity, respectively, and d indicates the thickness of the GSP layer.

	DAE1 (open form)	DAE2 (open form)	DAE3 (open form)
Tg	374 K (101°C)	379 K (106°C)	405 K (132°C)
Thickness dependence of surface potential & GSP slope	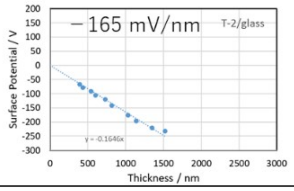	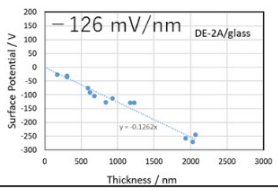	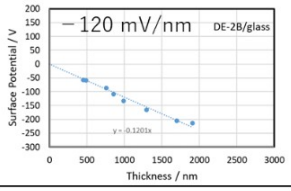
ε	2.7	2.9	3.0
PDM (D)	4.55	3.82	4.19
<cos θ>	−0.26	−0.22	−0.24

DAE4 (open form)	DAE11 (open form)	PTAA
320 K (47°C)	320 K (47°C)	343 K (70°C)
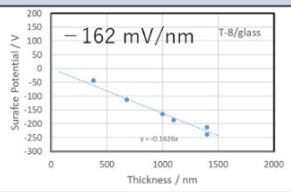	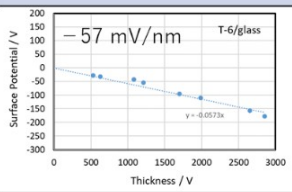	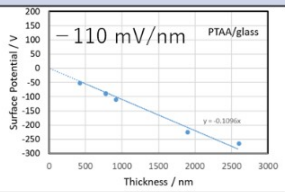
3.0	2.5	2.4
6.81	4.44	4.08
-0.14	−0.05	−0.15

Fig. S8 (a) Materials exhibiting negative GSP slope.

	DAE6 (open form)	DAE7 (open form)	DAE8 (open form)	DAE9 (open form)
Tg	293 K (20°C)	304 K (31°C)	305 K (32°C)	308 K (35°C)
Thickness dependence of surface potential & GSP slope	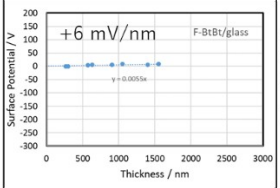	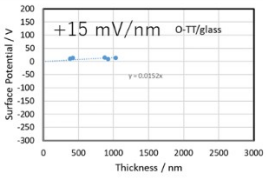	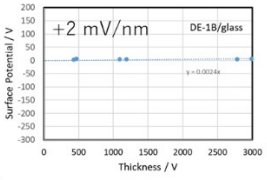	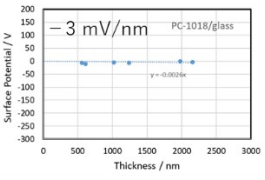
ε	3.2	3.2	2.6	3.4
PDM (D)	3.66	4.79	4.93	9.77
<cos θ>	0.01	0.01	0.00	0.00

Fig. S8 (b) Materials exhibiting nearly-zero GSP slope.

DAE	DAE10 (open form)	DAE5 (open form)	SPP (closed form)	Alq3 (reference)
Tg	343 K (70°C)	336 K (63°C)	327 K (54°C)	
Thickness dependence of surface potential & GSP slope	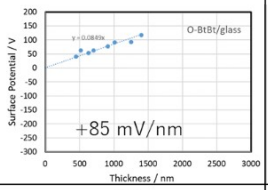	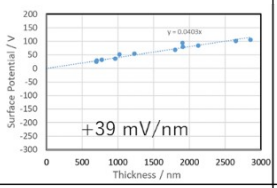	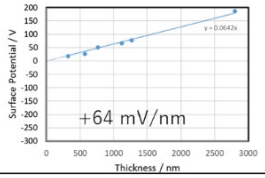	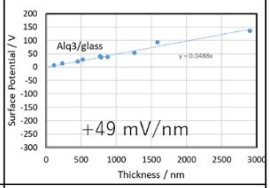
ε	2.7	2.2	2.8	-
PDM (D)	4.83	4.39	4.04	-
<cos θ>	0.05	0.04	0.05	-

Fig. S8 (c) Materials exhibiting positive GSP slope.

Correlation between GSP slope, PDM, and Tg

Figure S9a shows the relationship between PDM and the GSP slope. No clear correlation was observed in this analysis. In contrast, a distinct trend was observed between Tg and the GSP slope (Fig. S9b). Specifically, as Tg increased from around room temperature to approximately 130°C, the GSP slope also increased.

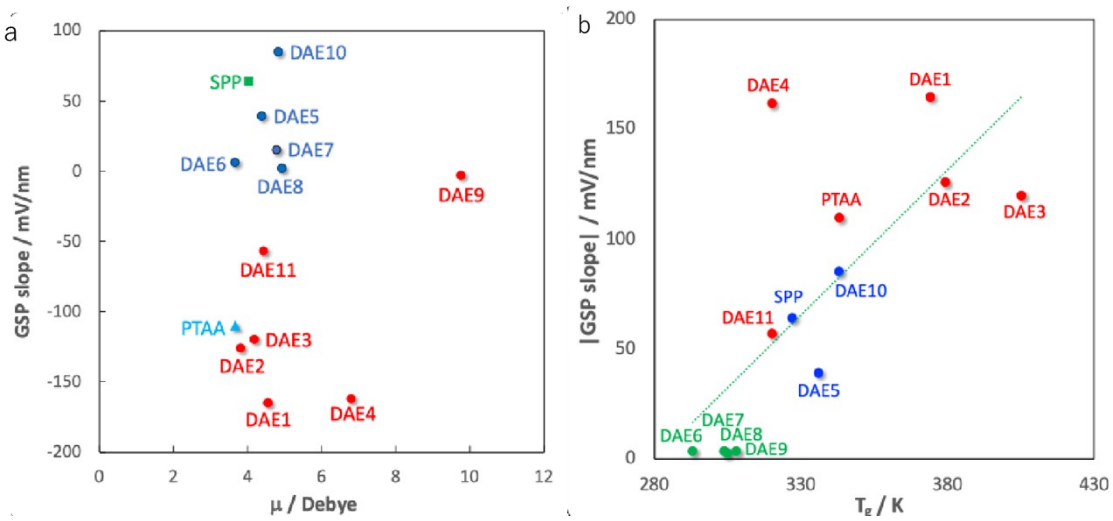

Fig. S9 (a) Correlation between PDM and GSP slope. The compounds were showed as positive GSP slope (blue cycles), negative GSP slope (red cycles), and two non-DAE compounds SPP (green square) and PTAA (cyan triangle), respectively. (b) Correlation between Tg and GSP slope. The materials were showed as positive GSP slope (blue cycles), nearly-zero GSP slope (green cycles) and negative GSP slope (red cycles), respectively. The dashed line is as a guide to the eye. (Reproduced from ref. 42. Copyright (2026) AIP Publishing)

Complicated movement of water droplet on GSP surface

The movement of the water droplet on the DAE5 surface is interesting (see Smovie5.mp4). The water droplet is “reflected” at the film edge, but is also “reflected” at the “track” where the water droplet passes, resulting in a very complicated movement. This is because the electric potential is reduced at the “track” of the water droplet. This type of movement also occurs on other GSP surfaces. The results also seem to indicate that droplets do not collide with other droplets and coalesce, although in exceptional cases, fast-moving droplets may coalesce due to inertia (see DAE5 in Smovie5.mp4).

Fig. S10 Complicated spontaneous movement of water droplet based on reduced surface potential of droplet “track”.

Absorption spectra of materials exhibiting GSP

Figure S11 shows the absorption spectra of the materials used in this study. Most of the materials used in this study exhibit absorption at λ = 365 nm, but PTAA does not. Therefore, we need to employ a shorter wavelength UV (λ = 254 nm) to investigate the photostability of the GSP of PTAA film.

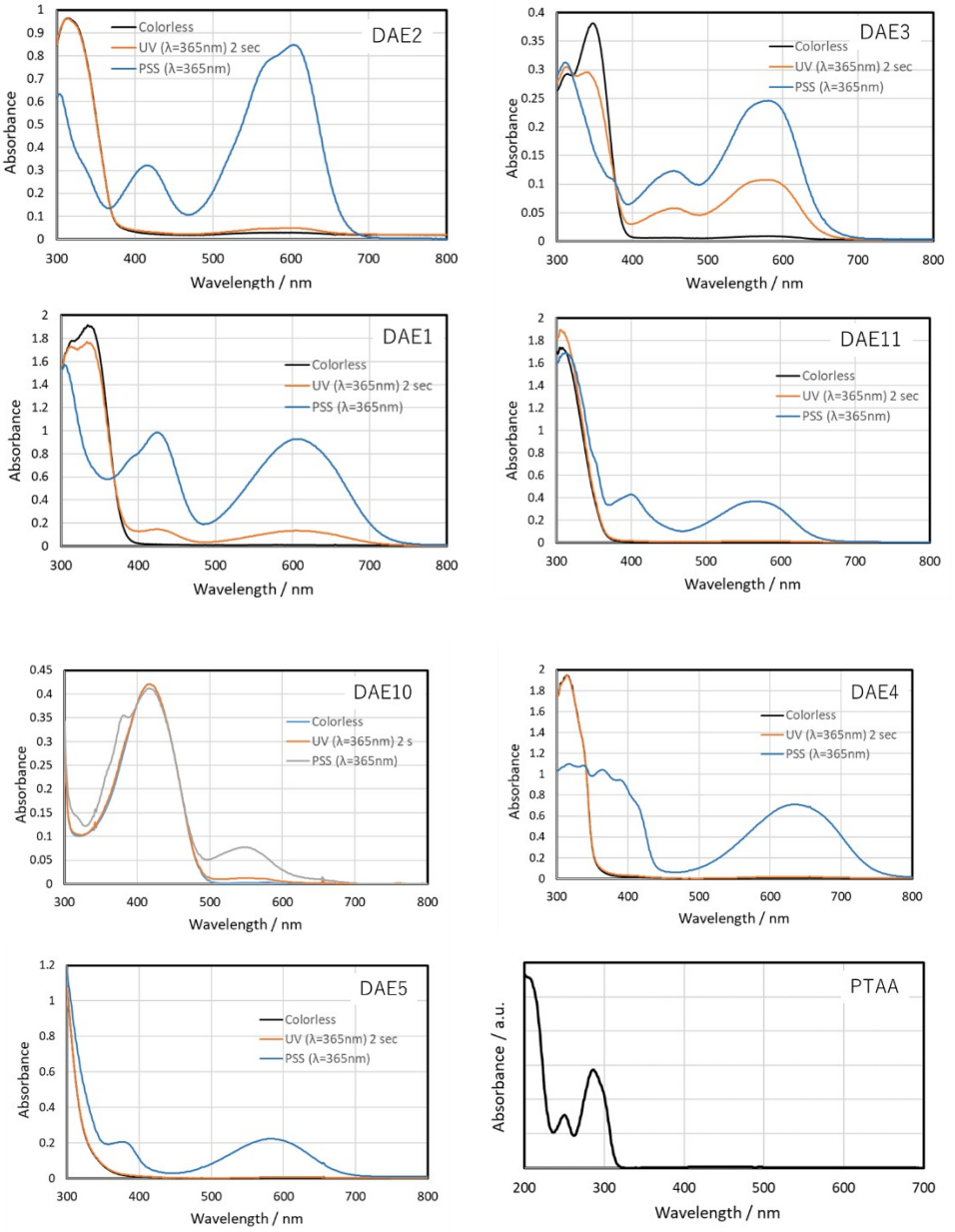

Fig. S11 Absorption spectra of materials (in toluene) exhibiting GSP.

Surface potential decrease upon UV irradiation (λ=365 nm)

Figure S12 shows the decrease in surface potential during UV irradiation with a wavelength of 365 nm, used to assess the stability of PTAA, DAE2, DAE5, and Alq3 (used as a reference sample). PTAA does not absorb at 365 nm. DAE2 exhibited a rapid decline in surface potential to zero within a few seconds, while Alq3 showed a decrease over tens of seconds. In contrast, PTAA and DAE5 demonstrated no significant decrease in surface potential even after 300 seconds of irradiation.

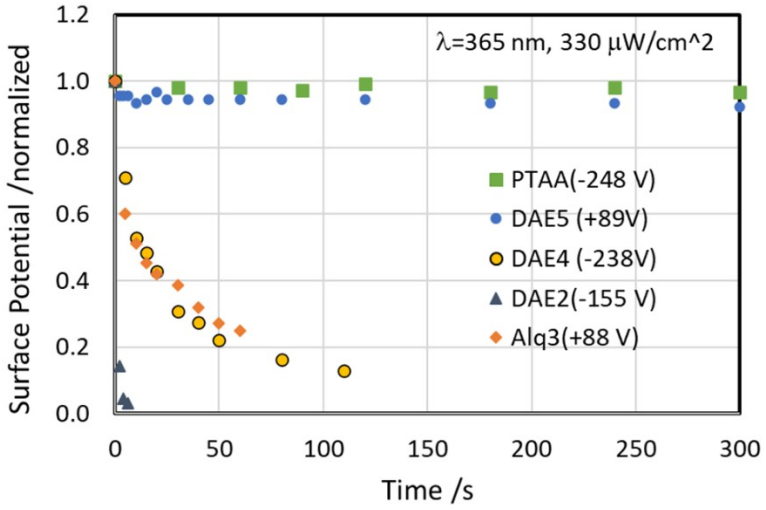

Fig. S12 Residual ratio of surface potential against UV irradiation (λ=365 nm). The initial potential is in brackets.

Dependence of GSP expression on substrate conductivity

When GSP materials were evaporated onto substrates, some did exhibit very low GSP slope on conductive substrates (Fig. S13). Notably, this includes DAE2, which showed a rapid decrease in surface potential upon UV exposure (Table S3). This drop is thought to be due to the inflow of carriers from the conductive substrate.

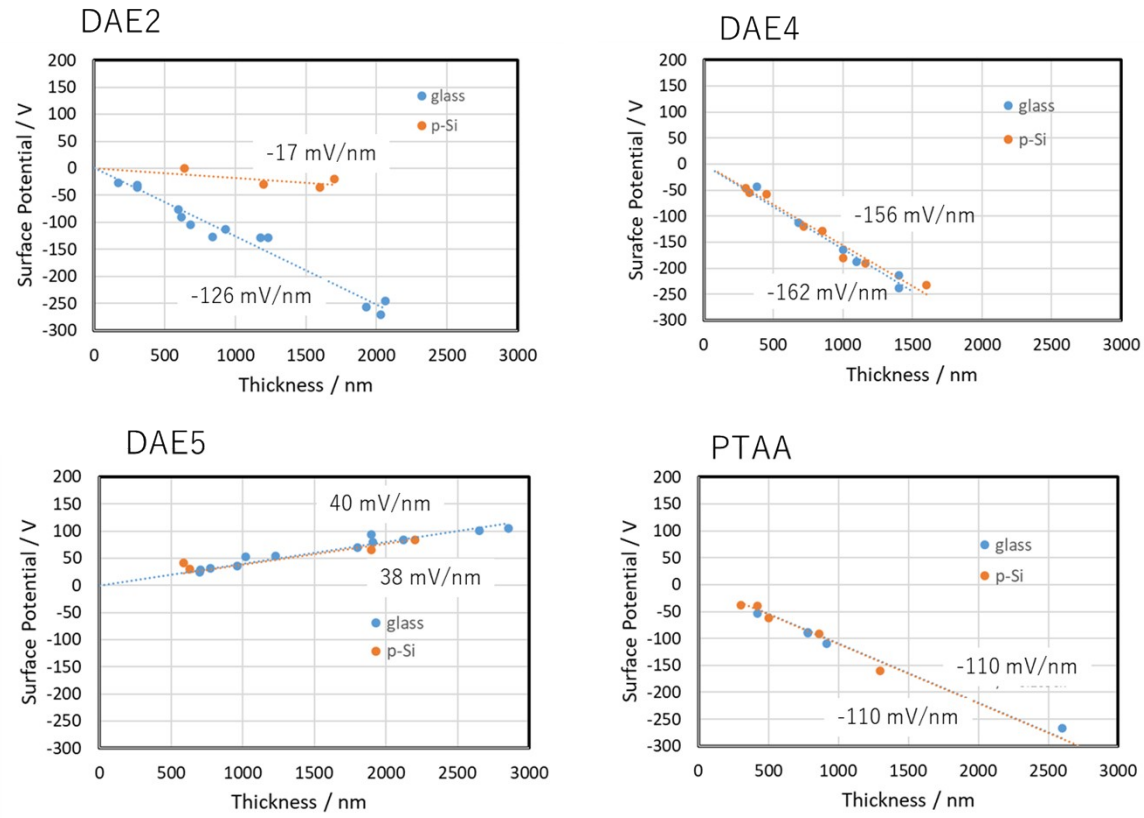

Fig. S13 Relationship between substrate conductivity and GSP slope.

Table S3 GSP tendency depending on substrate conductance and stability upon UV irradiation.

	DAE2	DAE3	DAE1	DAE11	DAE10	DAE5	PTAA
Glass:	-126 mV/nm	-120 mV/nm	-165 mV/nm	-57 mV/nm	+85 mV/nm	+40 mV/nm	-110 mV/nm
p-Si 10^3 Ω/sq.	-18 mV/nm (-18 mV/nm on Au/glass, -6 mV/nm on ITO)	-20 mV/nm	-69 mV/nm	-63 mV/nm	+86 mV/nm	+38 mV/nm	-110 mV/nm
Potentia decrease upon UV irradiation (λ =365 nm)	Rapid decrease	Rapid decrease	Rapid decrease	Decrease	Decrease	Stable	Stable (λ =254 nm)

Stability of GSP

Compared with other GSP materials, PTAA exhibits superior resistance not only to light but also to humidity. Figure S14 shows the change in surface potential of a PTAA film exhibiting GSP after being left in an air-conditioned room for approximately one month. After an initial 10% decrease—likely caused by ambient humidity—the surface potential remained at 90% of its initial value even after one month. Although the highly insulating DAE5 also demonstrated good humidity stability, the less insulating DAE2 and other films showed a relatively rapid decrease to less than half of their initial potential, suggesting that the insulating properties of the films play an important role in determining their stability.

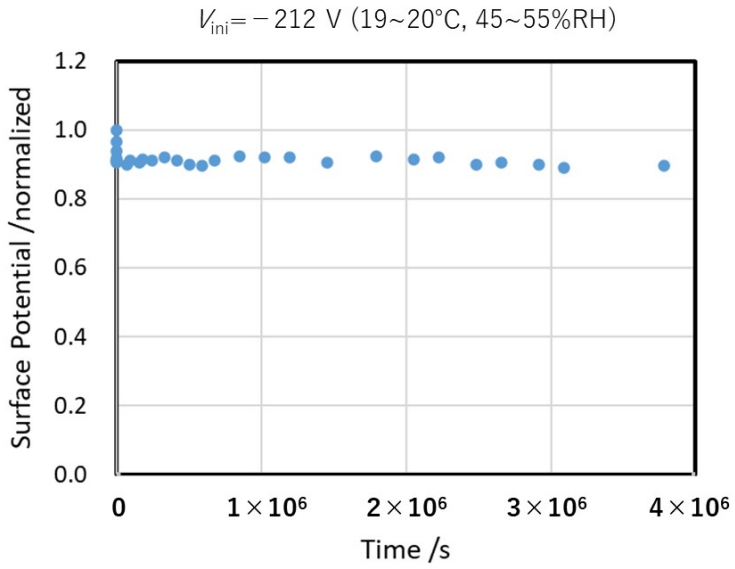

Fig. S14 Stability of GSP of PTAA film.

COSMO-RS solvation model and σ-profile

The Conductor-like screening model for real solvents (COSMO-RS) model originally developed by Andreas Klamt *et al.* [ref. 48,49], as an effective predictive model of thermophysical properties has attracted large interest in the recent years. The model is based upon density functional theory (DFT) calculations incorporating an implicit solvation model, the so-called conductor-like screening model (COSMO), which is similar to other polarizable continuum models (PCMs) but includes an additional outlying charge correction that goes beyond the cavity surface. The screening charge distribution (SCD) of a molecule embedded in a perfect conductor (with an infinitely large dielectric constant), then, can be obtained from the electrostatic potential of the molecular electron density for the molecule-shaped cavity. In COSMO-RS approach, the molecular surface is divided into a number of equal-area segments, and each segment of a surface has a surface charge density (*i.e.* the actual charge distribution averaged over segment area). Instead of calculating all the different mutual contacts of the three-dimensional (3D) representation of the molecule, a further simplification of the SCD is introduced by means of the SCD profile (so-called "σ-profile"): The charge distribution on the 3D molecular surface is reduced to a two-dimensional histogram, that represents the probability to find a certain SCD on the cavity surface of molecule. Based on the SCD information, the electrostatic and hydrogen bonding interactions based on SCD, as well as van der Waals interactions can be calculated assuming that each segment interacts independently. The approximation of independent surface segments makes the computation of thermodynamic ensemble properties quite tractable.

A representative example of the σ-profiles is shown in Fig. S15 for nonpolar hexane, benzene and polar water molecules. The entire σ-profile areas can be roughly divided into three regions; the electronic basicity region, the nonpolar region, and the electronic acidity region from negative to positive-σ range. As illustrated in Fig. S15, the σ-profile of water molecule has a

relatively broad distribution, with two almost symmetrical peaks in the negative and positive regions, attributed to two polar hydrogen and one oxygen atom, respectively. On the other hand, the nonpolar benzene molecule shows two symmetrical picks in the region slightly off center, where the pick in positive σ-region can be assigned to delocalized σ-electron in benzene. For hexane, there is a narrow distribution of a nearly neutral charge density around zero, with a shoulder appearing in slightly positive region arises from the carbon atoms of hexane.

The σ-profile quantifies the density distribution of charges of a given polarity on the molecular surface, which is used in conjunction with statistical thermodynamics to calculate the electrostatic interaction energy between pairs of surface segments. In fact, comparing the σ-profiles of two molecules can provide straightforward insights for estimating intermolecular compatibility based on their polarity. Table S4 summarizes the water droplet mobility and ΔG for each material.

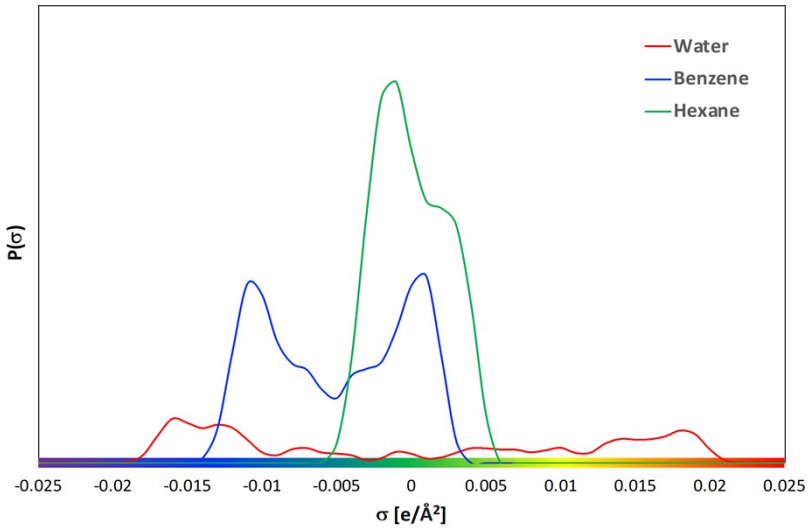

Fig. S15 Three representative σ-profiles of nonpolar (hexane, benzene), and polar (water) molecules.

Table S4 Summary of water-droplet mobility; surface roughness (Ra), and free energy in water (ΔG)

	DAE1	DAE2	DAE3	DAE4	DAE11	DAE10	DAE5	PTAA	Alq3
Droplet movement (observed)	NG	NG	NG	Fair	Fair	Fair	Fair	Excellent	NG
Ra < 1 nm T_g=323~343 K	NG T_g=374 K	NG T_g=379 K	NG T_g=286 K	Good T_g=320 K	Good T_g=320 K	Good T_g=343 K	Good T_g=336 K	Good T_g=343 K	NG T_g=378~450 K
ΔG in water (kcal/mol)	2.15	2.20	1.36	6.24	6.05	4.68	5.15	9.36	-0.24